Pergamon

Int. J. Heat Mass Transfer. Vol. 40, No. 11, pp. 2595–2605, 1997

Printed in Great Britain
0017–9310/97 $17.00+0.00

PII: S0017-9310(96)00284-0

Experimental study of natural convection in a model alloy with a miscibility gap

S. LÜNSKENS and J. N. KOSTER
University of Colorado, Department of Aerospace Engineering Sciences, Boulder, CO 80309-0429, U.S.A.

(*Received* 23 *April* 1996 *and in final form* 9 *August* 1996)

Abstract—To solidify a dispersion alloy with a miscibility gap in the liquid state, the two-phase immiscible region may have to be traversed. The composition and consequently the properties of the solid depend on the distribution of the minority dispersion phase. The distribution is mostly controlled by density segregation and convective flow in the melt. Natural convection in a transparent model alloy of 65 w% paraffin oil and 35 w% benzylbenzoate was investigated with LDV and holographic interferometry. The benzylbenzoate-rich dispersed phase is the heavier component. The lighter paraffin oil phase was the majority component. A horizontal temperature difference was applied to the liquid layer with the cold side temperature below the phase separation temperature and the hot temperature above it. The liquid system undergoes phase separation when approaching the cold wall and dissolution when approaching the hot wall. Flow velocities at different locations in the test cell are measured and compared to density field visualizations. At small temperature differences the natural convection flow is time-dependent, due to the phase separation process. © 1997 Elsevier Science Ltd. All rights reserved.

1. INTRODUCTION

The strength of metal alloys can be improved by the dispersion of fine particles in the matrix. There are two kinds of dispersion alloys: those formed with non-dissolving solid particles, and monotectic binary alloys with a miscibility gap in the liquid state. Typical dispersion alloys are the aluminum-based dispersion alloys composed of a majority matrix phase of aluminum and a minority phase of immiscible components such as graphite, bismuth or lead. They are used as dry bearing materials which do not require liquid lubrication; graphite, bismuth or lead play the role of lubricant. Graphite particles have high melting points and are thus dispersed in the solid state into the Al-melt. With the other elements, Bi, Pb, aluminum forms a monotectic phase diagram which has a region of liquid immiscibility above the monotectic temperature [1–4]. Here we focus on that class of alloys with liquid–liquid dispersions.

Typically these alloys are manufactured at the monotectic composition to avoid the liquid miscibility gap. The solid phase engulfs liquid drops that freeze only at much lower temperature. In industrial processes, however, it may happen that the concentration of elements is slightly off-monotectic, which leads to a two-phase formation in the melt. Furthermore, it may become of interest to solidify alloys at off-monotectic composition if improved physical properties are predicted. In this case the fluid mechanics of the two-phase melt needs to be understood.

The quality of these dispersion alloys is defined by the degree of homogeneity of the minority phase distribution. During the alloy solidification, the melt is subject to a temperature gradient. Temperature gradients in a gravity field lead in most cases to buoyancy driven convective flows. The temperature of the solidification front is below the two-phase region, but the hot temperature maybe in the two-phase region or still above the miscibility gap in the single phase region. Convective flow thus includes traversing the equilibrium temperature regions of single-phase liquid, two-phase liquid and solidification with liquid phase incorporation. The two-phase liquid consists of dispersed drops in a matrix liquid. As the concentration of elements is different in both phases, the minority phase may experience buoyancy or sedimentation. Convective flows tend to entrain dispersed droplets. Any sedimentation or buoyancy will have an influence on the flow pattern. Flow between hot and cold regions leads to a dynamic mass transfer, drop coalescence and formation and dissolution of the dispersed phase. Furthermore, at the liquid–liquid interfaces of the drops, thermocapillary forces may become contributors to the droplet distribution. In summary, the termo-fluidmechanic problem of miscibility gap alloy melts becomes extremely complex.

A major difficulty in investigating liquid metals is their opaqueness. Therefore, organic liquids are often used as model substances to study the flow and the solidification of alloys. One basic problem which has been studied to some extent is the migration of single and entrained drops in a fluid subject to a temperature gradient, in a gravity field, as well as under microgravity conditions [5, 6]. Furthermore, the issues of coalescence, growth and disappearance of drops in

NOMENCLATURE

A	aspect ratio $A = H/L$
BBO	benzylbenzoate
C	constant, equation (3)
c	concentration
D	depth of the test cell (visualization direction)
g	gravitational acceleration
H	height of the test cell
L	length of the test cell
PO	paraffin oil
Ra_c	critical Rayleigh number
Ra_H	Rayleigh number based on vertical temperature gradient
Ra_L	Rayleigh number for the natural convection problem
T_{cold}	temperature at the cold side of the test cell
T_{hot}	temperature at the hot side of the test cell
ΔT	temperature difference, $T_{hot} - T_{cold}$
x	axial distance at which the LDV profile is taken.

Greek symbols

β	thermal expansion coefficient
κ	thermal diffusivity
ν	kinematic viscosity.

isothermal liquids have been studied. The phase separation process, spinodal decomposition and nucleation are studied with and without flow under gravity, as well as microgravity conditions [7, 8].

Studies of convective flow in miscibility gap alloys are limited. Phase separation under natural convection was first reported by Platten and Chavepeyer [9]. It was shown that phase separation happens whenever the cold temperature is below the phase separation temperature. Flow visualization was provided by experiments performed with a binary mixture of benzylbenzoate (BBO) and paraffin oil (PO), using real time holographic interferometry, as well as Schlieren photography [10]. Their goal was the investigation of the natural convective flow and the separation process at different temperature gradients across the miscibility gap transition.

Although holographic interferometry and Schlieren photography give excellent field visualization, they do not give information about the flow velocity and the flow direction. The following experiment is intended to provide flow velocity data to compare with density fields. The procedure from [10] is adopted to ease comparisons.

2. EXPERIMENT

This work provides flow velocity measurements at different locations in a natural convection test cell. Velocities are then compared to Schlieren and density visualizations.

The test cell is a rectangular cavity. The cavity is formed from an aluminum plate whose center is milled into a rectangular opening. The back and the front of the cavity are confined by two vertical glass windows. The test cell is embedded in a large PVC frame for thermal insulation. A schematic of the cell is given in Fig. 1. The dimensions of the liquid layer are:

$$\text{Height}(H) \times \text{Length}(L) \times \text{Depth}(D) = 17.1 \times 38.1 \times 7.7\,\text{mm}.$$

The aspect ratio is $H/L = 0.45$; the fluid volume is 5.03 mm^3. Large aluminum cooling jackets are attached to the aluminum plate to achieve isothermal boundary conditions at the vertical endwalls of the liquid layer. Upper and lower horizontal boundaries are subject to linear temperature profiles. Temperature gradients are horizontal, thus, the induced cavity flow will be natural convection. Thermostats circulating coolant through the jackets and large brass thermal buffers provide a short-term temperature constancy of better than ± 0.01 K in the test cell. The endwall temperatures are measured with two thermocouples mounted in the vertical walls, approximately 1 mm away from the liquid.

Two measuring techniques are used: holographic interferometry for density field visualization, and laser Doppler velocimetry (LDV) for single component velocity measurements. Due to the nature of LDV, a fluid system with two compounds of equal refractive index would give the best results. No such system could be found, so the benzylbenzoate (BBO) from Aldrich, catalog # B1.770-0 and paraffin oil (PO) from Malinckrodt, catalog # 6357 (mineral oil, white, heavy), were used. The chosen solution was a 35 w% BBO-65 w% PO composition, where 'w%' stands for 'weight percent'. Both pure liquids and their solutions are transparent, relatively easy to handle, and not very toxic. Density and viscosity are different for the pure liquids (Table 1), which suggests segregation in a gravity field if the consolute line temperature is reached.

Although the phase diagram was determined earlier [10], the exact consolute temperature for the 35 w% BBO-65 w% PO mixture was checked separately, because another charge of paraffin oil was used in this study. The trend in density of the solutions can also

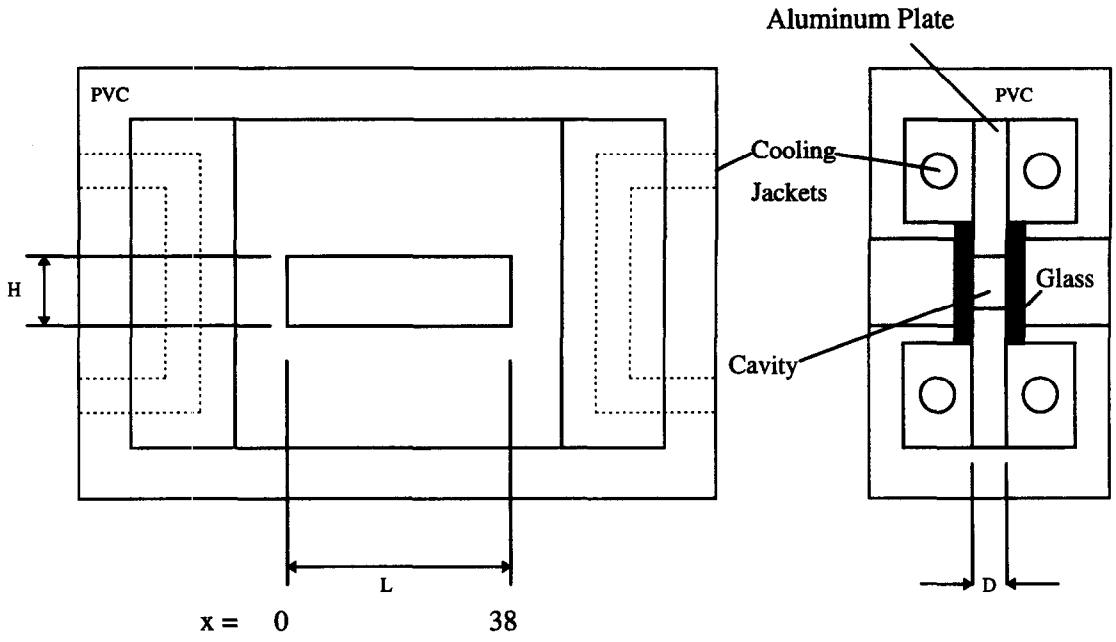

Fig. 1. Test cell.

be assessed from [10]. The mixture used for the measurements was placed in a glass tube at 35°C, well above the consolute line temperature and cooled down at a very low cooling rate of 1 K/h. The temperature when the liquid became disperse was approximately 27.5°C. To achieve the highest possible accuracy, the measurement was repeated in smaller steps of 0.2 K/h around the first detected separation temperature. 27.5°C was the exact separation temperature for the prepared 35 w% BBO-65 w% PO mixture.

LDV required the addition of particles to the liquids. These particles were custom designed to match the density of the liquids [11]. The silver-coating process started with Ecco-spheres SDT-60 by Emmerson and Cuming, Inc., size < 10 μm diameter and was done only once to achieve the density of the 35 w% BBO-65 w% PO composition at the temperature of $T = 30$°C.

The LDV system measures the horizontal velocity component of the seeded particles at one specified location in the test cell. The system takes 1024 data points and averages the velocity for this point. Then the traverse table moves the test cell 0.25 mm in the vertical direction to take the next 1024 data points. Under these conditions, mapping one vertical plane from the bottom to the top of the test cell at a specific location takes about 11 min. Figure 3 shows two velocity profiles at the same location ($x = 4$ mm) taken in a 45 min time interval. The profile change in that time interval is small so it can be assumed that changes during one 11 min profile mapping is negligible. After the velocity profile at one x-coordinate is taken, the traverse table moves to another location to start the next vertical velocity profile.

Table 1. Density, viscosity and boiling point of the liquids

	Benzylbenzoate	Paraffin oil
Density [g cm^{-3}]	1.118[a]	0.88[b]
Kinematic viscosity [cm^2 s^{-1}]	0.0761[c]	0.74–0.78[b]
Boiling point [°C]	323[c]	

[a] The Merck Index, 11th edn, 1989.
[b] Sigma Chemical Company, 1994.
[c] Dean, J. A., *Lange's Handbook of Chemistry*, 14th edn. McGraw-Hill, New York, 1992.

In order to initiate natural convection, the hot wall temperature is ramped to a set point above the consolute line temperature, and the cold wall temperature is ramped to a set point below the consolute temperature. The experiments are started with a 24 h isothermalization at 30°C. The temperature gradient of $\Delta T = 2$ K is established with a slow system ramping rate of 1 K h^{-1}. The measured end wall temperatures in the test cell were $T_{hot} = 28.5$°C (above the consolute), $T_{cold} = 26.5$°C (below the consolute) and left constant for the entire experiment.

At the hot side, the equilibrium condition of the fluid is the single fluid phase, whereas at the cold side, the equilibrium condition is the two-phase dispersed liquid. The consolute temperature is thus within the core fluid layer. The natural convective flow transports liquid from the hot side to the cold side. This flow leads to a liquid separation when flow is from hot to cold and dissolution when flow is from cold to hot.

No thermophysical data were available for the chosen composition. These data are required to calculate pertinent non-dimensional parameters. In order to evaluate the Rayleigh number, an indirect strategy

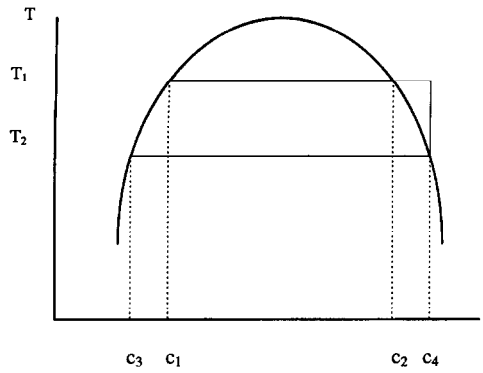

Fig. 2. Schematic phase diagram of the BBO/PO system. Refer to measured phase diagram in Ref. [10].

was developed to quantify the flow. Knowing the critical Rayleigh number in a liquid layer heated from below,

$$Ra_H = \frac{g\beta\Delta T H^3}{\nu\kappa} \quad (1)$$

the critical temperature difference for the onset of convection is measured. As the values of β, ν and κ are unknown for the investigated mixture, equation (1) is simplified to:

$$Ra_c = C\Delta T H^3 \quad (2)$$

where the thermophysical properties and the gravitational acceleration are combined in a constant C in units of $(m^3\,K)^{-1}$:

$$C = \frac{g\beta}{\nu\kappa}. \quad (3)$$

The experimental apparatus to test the stability of the liquid layer has the dimensions of $H \times D \times L = 10 \times 6 \times 200$ mm. Experiments are performed in the single phase region at the average temperature $T = 30°C$. For rigid–rigid boundary conditions, the critical Rayleigh number for such a confined layer in a box is $Ra_c = 3560$ [12], higher than the critical value for the infinite layer. With the measured critical temperature difference of $\Delta T_c = 1.6$ K for the onset of convection, the constant computes as $C = 2.2 * 10^9\ m^{-3}\,K^{-1}$.

To convert the Rayleigh number of [1] to the natural convection problem, it is necessary to introduce the direction of the temperature gradient $\Delta T/L$ via the aspect ratio $A = H/L$ and Ra_L is defined as :

$$Ra_L = Ra_H A = \frac{g\beta\Delta T H^3 A}{\nu\kappa} = C\Delta T H^3 A. \quad (4)$$

With the calculated constant C and the applied temperature difference of $\Delta T = 2$ K, the Rayleigh number for the following experiment is calculated as $Ra_L = 9.8 * 10^3$.

The holographic interferometry experiments were performed separately with the same liquid and under the same initial and experimental conditions as the LDV experiments. The measurement technique and the experimental procedure are described in Ref. [10]. The comparison, therefore, is not one-on-one, but flow patterns at specified time steps are quite comparable.

3. RESULTS

With the cold side temperature below the consolute temperature, a dispersion of immiscible drops forms in the liquid. When the liquid flows toward the hot side, set at above the consolute temperature, the dispersed drops dissolve as the solubility limit line is crossed. In such a situation, a dynamic process of dispersion formation and dissolution occurs within the natural convection roll cell. Below the consolute temperature, the solution of 65 w% PO and 35 w% BBO separates into a PO-rich majority phase and

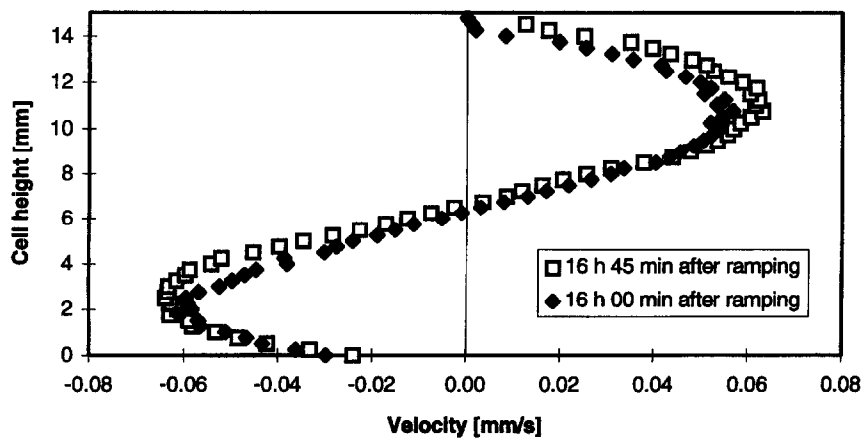

Fig. 3. Velocity profile at $x = 4$ at different times.

an immiscible BBO-rich minority (drop) phase. The composition of each phase is temperature-dependent according to the phase diagram. The initial BBO minority phase has a composition of about 15 w% PO. As the temperature is reduced further, the PO-rich majority phase can dissolve less BBO. The majority phase thus rejects BBO and becomes lighter (compare [10], Fig. 2). At the same time the BBO-rich drop phase dissolves less PO and becomes heavier.

Due to the scattering of laser light, interferograms do not give information in a fluid where a large number of dispersed fine droplets form a mist. LDV measurements, on the other hand, are possible since a small number of fine drops also act as tracer particles traversing the measurement volume. With time, the small droplets coalesce and the light dispersion mist disappears.

In the following interferograms, the left side represents the hot wall and the right side, the cold wall. Figure 4(a, b) were both taken directly after the end of the initial ramping to $Ra_L = 9.8 * 10^3$ ($\Delta T = 2$ K). The dark area in the interferogram represents the region of the droplets which disperse light. The vertical line through the interferogram indicates the plane of the velocity profile in Fig. 4(b). Although dispersions formed readily near the cold wall, the flow is composed of a single convective roll cell. The maximum flow velocity is of order 0.1 mm s^{-1}. This convective roll cell entrains the dispersed drops back toward the hot side wall where they dissolve. In Fig. 4(c, d) about 6 h 30 min into the temperature plateau, the gravitational separation of the dispersed and majority phase has started. The velocity profile indicates one convective roll cell in the lower dispersed region. The separation reduces the flow velocity substantially.

To understand the visualization in Fig. 4(c), a close look at a schematic phase diagram (Fig. 2) is necessary. During the convective flow from the hot to the cold side, a PO-rich majority phase is formed (composition c_2) as heavier BBO-rich droplets of the composition c_1 are rejected and sediment due to gravity. At the cold wall, the lighter, highly viscous PO-rich majority phase with the lighter composition c_4 segregates and floats on top of the convecting bulk liquid. In this upper portion the velocity data show liquid stratification and weak or stagnant flow. The *decrease* of the density of the majority PO-phase liquid due to the formation of the higher density dispersed BBO-phase is counteracted by the *increase* of density due to the lower temperature at the cold side. The decrease is larger than the increase; consequently the liquid with the composition c_4 rises at the cold wall where it becomes stagnant. Given sufficient time, the liquid of concentration c_4 will mix with the convecting liquid below the Schlieren at concentration c_2 and therefore disappear with time. In addition, the majority PO-phase increases its viscosity as BBO-rich liquid is rejected [10], which explains the reduced flow velocities.

Figure 4(e, f, g) (about 28 h into plateau) show a more complex flow pattern. The interferogram shows four main regions separated by concentration Schlieren. Figure 4(g) is the vertical velocity profile taken at $x = 11.5$ mm, represented by the left line in Fig. 4(e). Note that only the horizontal components of the velocity vector are measured. Higher velocities may exist at an angle to the horizontal plane. A convective roll is suspended between two stagnant regions that are bound by concentration Schlieren in the interferogram. The interferogram shows density stratification in the bottom layer. The roll cell is confined locally between the concentrational Schlieren visualized in the interferogram. The LDV measurements along the plane next to the cold wall ($x = 26.5$ mm, Fig. 4(f)) show that the convection in the lower region is bound by a no-flow region at the top. In the interferogram this separation is viewed as an upper concentrational Schlieren. Above the Schlieren, in the upper right corner, flow is very slow. From the development of that corner region as shown in Fig. 4(c), the liquid in this region is expected to have a highly viscous PO-phase of concentration c_4 that is slowly mixed with PO-majority phase of concentration c_2. At the very bottom, where a Schlieren and stratification (horizontal fringes) is observed in the interferogram, the velocity profile is perturbed.

Approximately thirty four hours into the plateau the Schlieren pattern has changed (Fig. 5(a, b, c)). A corner region at the cold side with visible dispersion drops remains stationary. This liquid appears to be the viscous PO majority phase of concentration c_4 developing from the situation in Fig. 4(c). The LDV profile (Fig. 5(b)) shows higher dispersion related scattering of velocity in that area, but one roll cell is still visualized in the region between the two slanted concentrational Schlieren in the middle region (Fig. 5(c)). The velocity profile indicates a weak flow in the upper part of the layer (Fig. 5(c)) where the concentrational Schlieren is traversed, in agreement with the interferogram. Another convection roll cell is at the hot wall and limited by the Schlieren to the right. No LDV data were taken in that region.

At around 42 h (Fig. 5(d, e)), a precipitate of droplets remains visible at the cold (right) side. The area with the PO majority phase of concentration c_4 in the upper right corner of Fig. 5(a) became smaller and eventually vanished a couple of hours later (Fig. 5(f), taken at 48 h 30 min after ramping). Along the bottom wall not all of the dispersed BBO-rich fluid dissolved on its way to the hot side. The coalescence of BBO-rich droplets led to a sedimentation layer of BBO-rich liquid at the bottom of the cavity. This layer, replenished at the cold side, dissolved continuously at the lower left (hot) corner and locally increased the density, attenuating the buoyant upflow. The flow profile (Fig. 5(e)) shows a roll cell in the lower part and another one with the opposite flow direction in the upper part. A Schlieren line is crossing the velocity plane. The strong scattering of the velocity values

a) directly after ramping

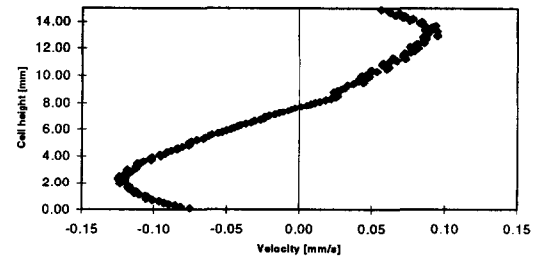

b) directly after ramping, x = 19 mm

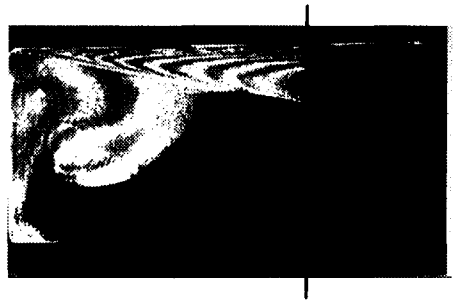

c) 6 h 30 min

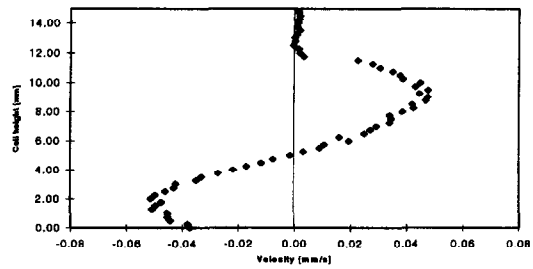

d) 6 h 33 min, x = 26.5 mm

e) 28 h

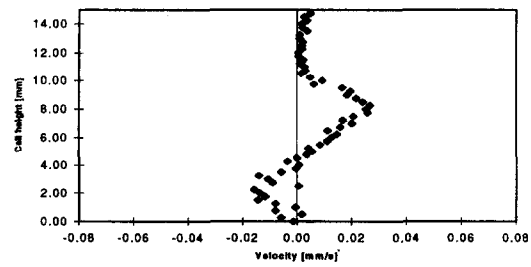

f) 27 h 47 min, x = 26.5 mm

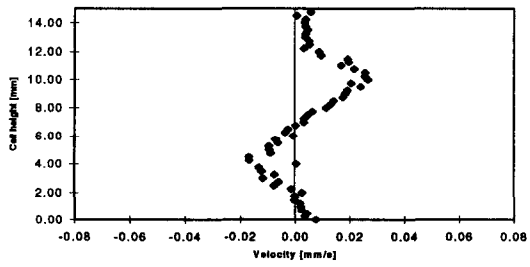

g) 28 h 31 min, x = 11.5 mm

Fig. 4. (a) Interferogram directly after ramping (line = 19 mm); (b) flow profile directly after ramping at $x = 19$ mm; (c) interferogram 6 h 30 min after ramping (line = 26.5 mm); (d) velocity profile 6 h 33 min after ramping at $x = 26.5$ mm; (e) interferogram 28 h after ramping (left line = 11.5 mm, right line = 26.5 mm); (f) velocity profile 27 h 47 min after ramping at $x = 26.5$; (g) velocity profile 28 h 31 min after ramping at $x = 11.5$ mm.

a) 34 h 30 min

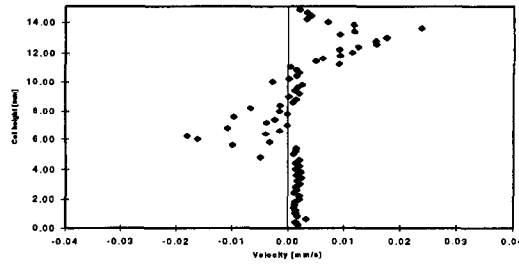

b) 33 h 10 min, x = 31.5 mm

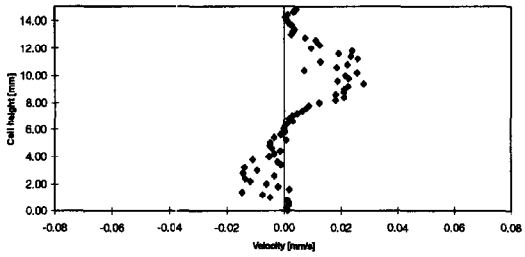

c) 34 h 50 min, x = 21.5 mm

d) 43 h 30 min

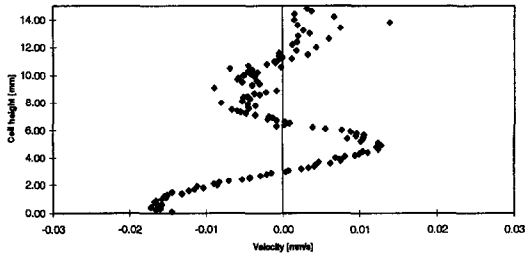

e) 42 h, x = 11.5 mm

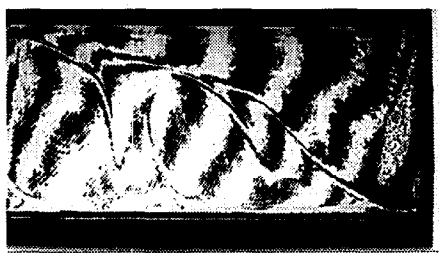

f) 48 h 30 min

Fig. 5. (a) Interferogram 34 h 30 min after ramping (left line = 21.5 mm, right line = 31.5 mm); (b) velocity profile 33 h 10 min after ramping at $x = 31.5$; (c) velocity profile 34 h 50 min after ramping at $x = 11.5$ mm. Velocity profile 33 h 10 min after ramping at $x = 31.5$; (d) interferogram 43 h 30 min after ramping (line = 11.5 mm); (e) velocity profile 42 h after ramping at $x = 11.5$ mm; (f) interferogram 48 h 30 min after ramping.

indicates more and larger dispersed droplets in the upper region.

At about 55 h (Fig. 6(a)), the isodensity lines indicate a convective roll at the right upper corner, as well as close to the hot wall. In the middle, a dynamic flow of dispersions and concentration gradients indicate mass transfer between the roll cells. The concentrational Schlieren extend across the diagonal of the cavity. Figure 6(b) shows a very weak flow in the lower part and an unclear flow situation in the upper part. The dispersed drops limit the accuracy of the velocity measurements in the upper area. Figure 6(c) shows the same pattern as Fig. 6(b), although the interferogram (Fig. 6(a)) indicates a larger roll cell in the area of the $x = 6.5$ mm plane. The liquid descends along the bounding Schlieren line. In the upper part the flow velocity measurements deliver highly scattered data.

Reaching 63 h, Fig. 6(d, e, f, g) show one roll cell in the upper right portion and lower left area of the test chamber. There is still precipitation of droplets at the right side. The BBO-rich area in the lower left corner also still exists. Above it, a more uniform region exhibits convection. The flow profile at the hot side (Fig. 6(f)) shows the roll cell and also scattering at 10 mm cell height where the two diagonal Schlieren lines meet, separating the convection from flow in the upper region. In the center plane the flow profile (Fig. 6(g)) shows a roll cell in the upper part which is slightly perturbed due to the dynamic separation process. The middle area is even more perturbed, in agreement with the interferogram showing circular density patterns in this region. The convective flow in the plane $x = 26.5$ mm (Fig. 6(e)) at the right side is well developed and vigorous. At the bottom of the plane a Schlieren is traversed, below which the flow is stagnant.

At 65 h into plateau (Fig. 7(a)), a vertical Schlieren line that originates at the upper left corner migrates toward the cold side (Fig. 7(b)). Now there are three main and distinguishable areas bound by concentrational Schlieren. In the right corner, flow is toward the cold side where the liquid descends and droplets of the heavier dispersed BBO-rich minority phase are still rejected from the solution. The lower region of the cavity is BBO rich. It spreads out along the bottom of the test chamber. At the hot side the ascending liquid dissolves the BBO-rich phase and increases in density. The fluid in the upper part of the test chamber, which is flowing toward the cold wall, loses heat on its way. This fluid thus increases in density, resulting in downflow and recirculation in the middle of the cavity.

Figure 7(c, d, e, f) emphasizes the dynamics of the process. The lower stratified layer from Fig. 7(b) disappeared in Fig. 7(c). The velocity profile in the middle of the test chamber (Fig. 7(d)) shows a convective roll cell which is suspended in the liquid layer and is bounded on top and at the bottom by regions of almost stagnant liquid. Interferograms and velocity measurements do not correlate well in timing but both show different stages of the same situation. At the 11.5 mm plane (Fig. 7(e)) one roll cell extends from the bottom to the top. At the cold side (Fig. 7(f)) one roll cell can be detected. That roll is confined to the cold wall region between the end wall and the first Schlieren to its left.

The flow pattern dynamics continues. At approximately 144 h into the plateau (Fig. 7(g)), the interference pattern adopts a pattern similar to the one observed at 33 h into the plateau (Fig. 7(h), cf. Fig. 5(a)). The shape of the interference fringe pattern is very similar at both times. These figures indicate that the oscillation period of the natural convective flow at $Ra_L = 9.8 * 10^3$ ($\Delta T = 2$ K) can be estimated at 110 ± 10 h, which is close to the findings in Ref. [10].

Unknown is the cause of the slow oscillations at small Rayleigh numbers. Supporting experiments showed that under the same experimental conditions and in pure BBO, steady natural convection (Equation (4)) develops without any oscillation up to $Ra_L = 9.8 * 10^5$ ($\Delta T = 5$ K, $C = 8.9 * 10^9$ m^{-3} K^{-1} (Equation (3)). As the viscosity of PO is much higher than BBO, no additional experiments with that fluid were required. The oscillating convection is found to be caused by the dynamic phase separation and dissolution processes during natural convection.

4. CONCLUSION

We studied natural convection in a binary model alloy undergoing liquid–liquid phase separation. The dynamic phase separation and dissolution process leads to a very complex time-dependent flow pattern. Multiple roll cells dynamically form and disappear in the liquid layer. The convective rolls are sometimes suspended between stagnant layers. Concentrational Schlieren are found to delimit regions of single roll cells. The density change due to the phase separation and dissolution, is complemented by changes in viscosity. These changes attenuate the natural convective flow which is driven by the change of density as a function of temperature. There is a time-dependent appearance and disappearance of regions of liquids with both a different composition and different content of dispersed phase. A liquid stratification was never as permanent nor as totally horizontal as in the case of totally immiscible fluids [13]. The time-dependence of the convective flow appears to be related to the flow velocity, which is fast with respect to the slow diffusion rate and the dynamics of dispersion formation and dissolution.

The parameter space of convection in liquids with a miscibility gap is enormous. A theoretical model to describe such a flow is not yet available. The problem poses great challenges for modeling as it involves: (1) phase separation with mass transfer; (2) single-phase flow close to the hot wall and two-phase flow close to the cold wall; (3) complex density fields combined

a) 56 h

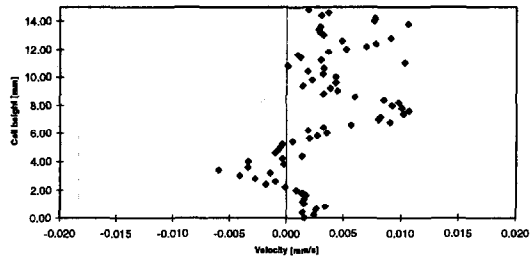

b) 55 h 50 min, x = 14.5 mm

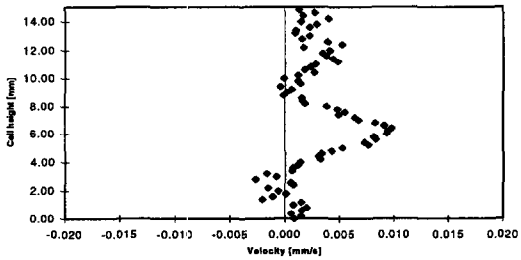

c) 55 h, x = 6.5 mm

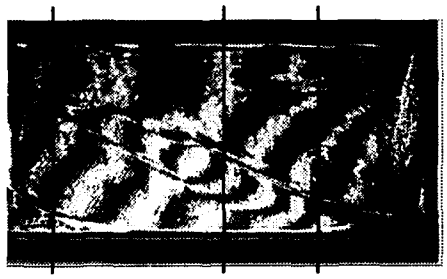

d) 63 h

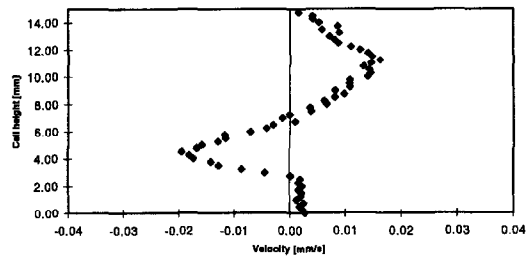

e) 62 h 51 min, x = 26.5 mm

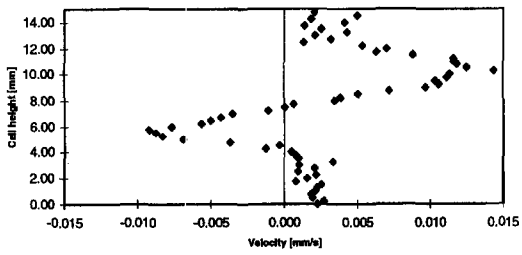

f) 63 h 55 min, x = 4 mm

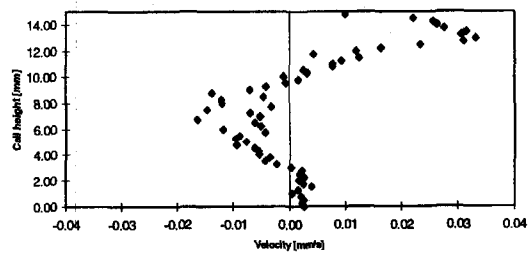

g) 63 h 13 min, x = 19 mm

Fig. 6. (a) Interferogram 56 h after ramping (left line = 6.5 mm, right line = 14.5 mm); (b) velocity profile 55 h 50 min after ramping at $x = 14.5$ mm; (c) velocity profile 55 h after ramping at $x = 6.5$ mm; (d) interferogram 63 h after ramping (left line = 4 mm, middle line = 19 mm, right line = 26.5 mm); (e) velocity profile 62 h 51 min after ramping at 26.5 mm; (f) velocity profile 36 h 55 min after ramping at $x = 4$ mm; (g) velocity profile 63 h 13 min after ramping at $x = 19$ mm.

a) 65 h

b) 70 h 30 min

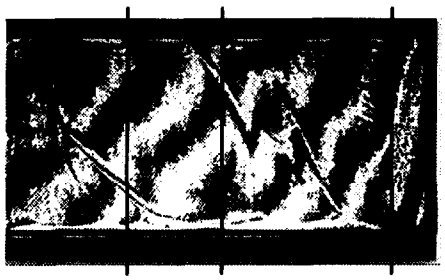

c) 75 h 30 min

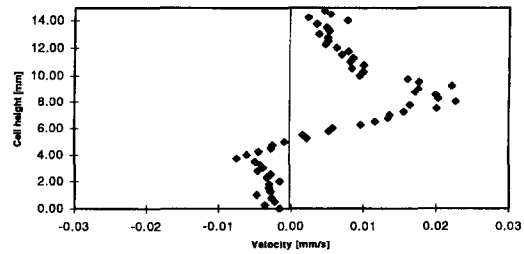

d) 76 h, x = 19 mm

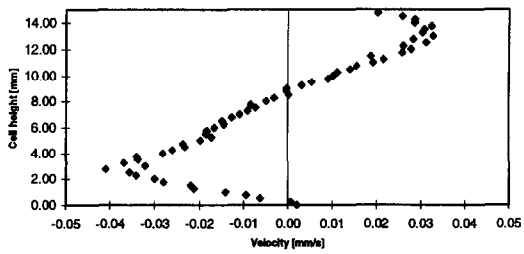

e) 76 h 11 min, x = 11.5 mm

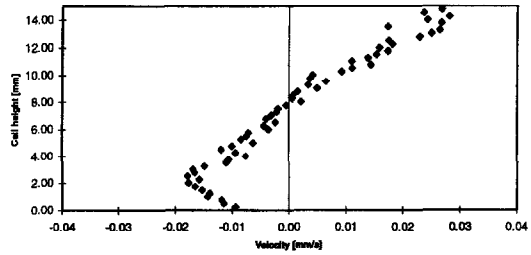

f) 75 h 38 min, x = 34 mm

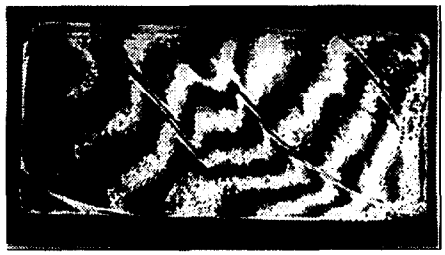

g) 144h 36 min

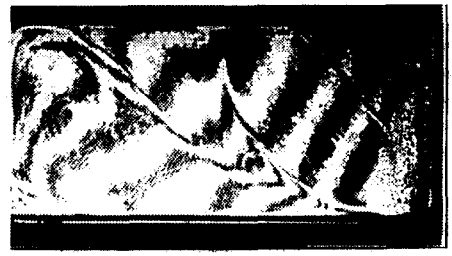

h) 33 h 30 min

Fig. 7. (a) Interferogram 65 h after ramping; (b) interferogram 70 h 30 min after ramping; (c) interferogram 75 h 30 min after ramping (left line = 11.5 mm, middle line = 19 mm, right line = 34 mm); (d) velocity profile 76 h after ramping at $x = 19$ mm; (e) velocity profile 76 h 11 min after ramping at $x = 11.5$ mm; (f) velocity profile 75 h 38 min after ramping at $x = 34$ mm; (g) interferogram 144 h 36 min after ramping; (h) interferogram 33 h 30 min after ramping.

with abrupt changes in viscosity; and (4) thermosolutal flow in the single liquid phases.

Acknowledgments—One of the authors (S.L.) gratefully acknowledges the financial support of the European Space Agency through a postdoctoral fellowship. Partial support under NASA grant NAG3-1094 is appreciated.

REFERENCES

1. Walter, H. U., Preparation of dispersion alloys—component separation during cooling and solidification of dispersions of immiscible alloys. *Proceedings of Workshop on Effect of Gravity on Solidification of Immiscible Alloys, Stockholm*, ESA SP-219, 1984, pp. 47–64.
2. Predel, B., Ratke, L. and Frediksson, H., In *Fluid Sciences and Material Science in Space: A European Perspective*, ed. H. U. Walter. Springer, New York, 1987, pp. 517–565.
3. Walter, H. U., In *Material Sciences in Space*, ed. B. Feuerbacher, H. Hamacher and R. J. Naumann. Springer, New York, 1986, pp. 343–378.
4. Reger, J. L., Interim Report on NASA Contract NAS8-28267, TRW Systems Group, Redondo Beach, CA, May 1973.
5. Merritt, R. M., Morton, D.S. and Subramanian, R. S., Flow structures in bubble migration under the combined action of buoyancy and thermocapillarity. *Journal of Colloid and Interface Science*, 1993, **155**, 200–29.
6. Merritt, R. M. and Subramanian, R. S., The migration of isolated gas bubbles in a vertical temperature gradient. *Journal of Colloid and Interface Science*, 1988, **125**, 333–339.
7. Beysens, D., Stability of critical fluid mixtures: experimental simulation of micro-gravity conditions. *Acta Astonautica*, 1985, **12**(7/8), 525–530.
8. Onuki, A., Spinodal decomposition and nucleation in the presence of flow. *International Journal of Thermophysics*, 1989, **10**(2), 293–308.
9. Platten, J. K. and Chavepeyer, G., Phase separation in nonequilibrium conditions. *Physics Letters*, 1993, **A174**, 325–328.
10. Koster, J. N. and Junior, V., Natural convection in a miscibility gap model alloy. *Journal of Material Synthesis and Processing*, 1994, **2**(6), 395–406.
11. Schmitt, T., Koster, J. N. and Hamacher, H., Particle design for displacement tracking velocimetry. *Measurement Science Technology*, 1995, **6**, 682–689.
12. Merker, G. P., *Konvektive Wärmeübertragung*. Springer, Berlin, 1987, pp. 359–369.
13. Prakash, A. and Koster, J. N., Convection in multiple layers of immiscible liquids in a shallow cavity. *International Journal of Multiphase Flow*, 1994, **20**(2), 383–396.